Huygens (and others) revisited

Kurt Wiesenfeld and Daniel Borrero-Echeverry
Center for Nonlinear Science and School of Physics, Georgia Institute of Technology, 837 State Street, Atlanta, Georgia 30332-0430, USA

We develop a generic iterative map model of coupled oscillators based on simple physical processes common to many such systems. The model allows us to understand, from a unified perspective, the range of different outcomes reported for experiments by Huygens and modern realizations of his two coupled clocks. © *2011 American Institute of Physics.*
[doi:10.1063/1.3665201]

In recent years, studies on complex systems have often centered on emergent behavior: cooperative interactions among the parts of the system lead to organized (and sometimes unexpected) behavior of the whole. The phenomenon of spontaneous mutual synchronization offers perhaps the most primitive example of emergent behavior. Synchronization is widespread in nature[1] and is relevant to many applications.[2] Intense efforts have led to substantial progress in understanding synchronization,[3] though open problems remain. This is so even for the simple case of two mechanical oscillators (e.g., pendulum clocks), where studies on similar realizations have reported qualitatively different outcomes. Our goal is to understand the source of these different results from a unified theoretical perspective.

I. INTRODUCTION

After his initial serendipitous discovery of antiphase synchronization of two pendulum clocks in 1665, Huygens systematically studied the phenomenon by mounting the clocks on a common supporting beam which itself was supported on the backs of two chairs.[4,5] Without exception, whenever the clocks fell into a synchronized state, the pendulums swung in antiphase. Huygens deduced that the key interaction was due to small movements of the supporting beam.

In an effort to recreate Huygens' system, Bennett *et al.*[6] built an apparatus consisting of two clocks mounted on a common rigid support, the support being constrained to move in one dimension along an air track (see Fig. 1). Here, too, the only synchronized state observed was the antiphase state. These observations were in agreement with simulations of the associated equations of motion.

Concurrently, Pantaleone carried out experiments on a very similar system, with mechanical metronomes instead of clocks; instead of an airtrack, the common supporting platform rested on smooth cylinders to allow low-friction translation in one dimension.[7] The metronomes almost always synchronized in-phase, with antiphase motion observed "only under special circumstances." His theoretical analysis agreed with the observations, as did subsequent simulations reported by Ulrichs *et al.*[8]

In an effort to understand the physical mechanism behind Huygens' antiphase observations, Dilão considered a model of two small-amplitude pendulums connected (between their pivots) by a spring-and-dashpot element.[9] He found that the damping strength of the dashpot controlled the asymptotic dynamics. For low values, both in-phase and antiphase states were stable; for larger values, only the antiphase state was stable. The latter case is consistent with Pantaleone's observations: one of the special circumstances where his metronomes locked into the antiphase state was when the cylinders rolled on a wet surface, which greatly increased the damping strength.[7]

Other recent research has explored a broader range of dynamical states for these (and closely related) systems. For example, Czolczynski and co-workers[10–12] ran simulations of two identical coupled pendulums and reported coexisting in-phase and antiphase attractors, but when the pendulums had unequal masses, they also observed a new periodic state in which the phase difference was itself periodic in time and commensurate with the faster oscillation period. They also reported chaotic states. In simulations of up to 30 oscillators, they described a variety of clustered states where subsets of oscillators were mutually synchronized. Their experiments using 11 metronomes showed synchronized, non-synchronized, and clustered states. Pantaleone also reported robust in-phase synchronization in experiments using seven metronomes.[7] Simulations by Ulrichs *et al.*[8] on up to 100 metronomes also show complicated (chaotic and hyperchaotic) behavior.

In this paper, we are concerned with the simplest possible observations of in-phase and antiphase synchronization, as typified by the experiments of Huygens, Bennett *et al.*, and Pantaleone. It may be that the differences in observed behavior are the result of differences in the detailed physics (e.g., choice of escapement mechanism), but the view we take here is that these systems are fundamentally the same, involving a single set of basic physical processes. We seek to understand the differing behaviors in terms of the relative importance of these processes.

Our approach is to develop an iterative map that incorporates a few simple effects common to many coupled nonlinear oscillator systems. We postulate that these effects are
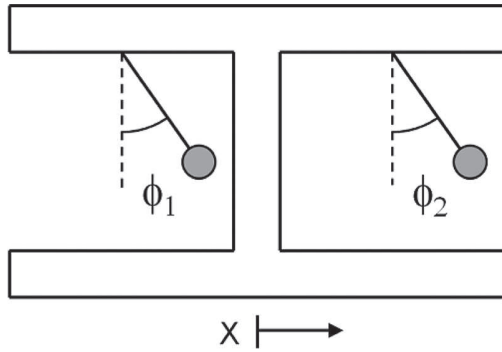
FIG. 1. Schematic of the system of coupled pendulums.

the dominant ones needed to determine the dynamical selection of one or the other phase-locked state. The map is simple enough that we can derive explicit expressions for the stability boundaries of the in-phase and antiphase states; it is general enough to encompass systems other than the mechanical ones that originally motivated it.

Our findings provide a straightforward explanation for the difference between the observations of Huygens (and Bennett *et al.*) and Pantaleone: the difference in observed behavior is attributable to differences in the relative importance of the main physical effects. The map also agrees well with numerical simulations of the differential equations of motion. In addition, we are led to a number of other predictions that could be tested by future experiments.

II. MAP DESCRIPTION

A. Single element

First, consider a single element. We have in mind an impact-driven oscillator, such as a mechanical clock or metronome, though we are not concerned with precisely capturing the details of the escapement mechanism. In between impulses, the oscillator evolves freely with frequency Ω. This may be represented by a rotating complex phasor z:

$$z \rightarrow z e^{i\Omega t}.$$

This motion is typically damped, so we take Ω to be complex. Since the oscillator is nonlinear, Ω typically depends on the amplitude. Occasionally, the oscillator gets an impulsive kick, whose effect is described by the map

$$z \rightarrow \gamma z + c \frac{z}{|z|},$$

where $0 < \gamma \leq 1$ and $0 < c < 1$. This generates a stable periodic orbit. Our choice of impulse map assumes that the kick affects the oscillator's amplitude but not its phase. This would be true, e.g., for a pendulum kicked at its lowest point. The form of the impulse rule is motivated by the two-part action of the escapement mechanism used in metronomes[10] and pendulum clocks,[6,13] which slow the oscillator upon engagement and then provide a fixed impulse.

Concatenating these two maps yields the full return map after a fixed time T (to be specified below):

$$z \rightarrow \left(\gamma z + c \frac{z}{|z|}\right) e^{i\Omega T}.$$

It will be convenient to express the frequency as the sum of the low-amplitude (constant) "linear" frequency ω and a "correction" due to nonlinearity. Specifically, we write

$$\Omega T = \omega T + f(|z|),$$

where f is the phase advance after a time T due to the amplitude-dependent frequency shift. For example, a pendulum's frequency decreases with amplitude, so the function $f(|z|)$ is a negative, monotonically decreasing function. The return map now reads

$$z \rightarrow \left(\gamma z + c \frac{z}{|z|}\right) e^{i\omega T} e^{if(|z|)}.$$

We choose T to be the oscillation period, whose value can be determined by finding the fixed point(s) z_0 of the map. In particular, letting $z_0 = \rho_0 e^{i\theta_0}$ and $\omega = \mu + i\nu$, where ρ_0, θ_0, μ, and ν are real numbers, results in the following system of coupled equations:

$$\rho_0 = (\gamma \rho_0 + c) e^{-\nu T}$$
$$\theta_0 = \theta_0 + \mu T + f(\rho_0) - 2\pi.$$

These equations can then be solved to determine T and ρ_0. The phase θ_0 remains undetermined, as expected for the map of an autonomous oscillator.

B. Coupled elements

For two or more coupled elements, we need to modify the free propagation rule. We assume the amplitude-dependent nonlinearity is weak enough that, to leading order, the system has independent normal modes. Writing z_j for the phasor of the jth oscillator, we introduce the normal mode coordinates $\{q_j\}$:

$$q_j = \sum_k S_{jk} z_k,$$

so that during free propagation each mode advances with the corresponding normal mode frequency ω_j:

$$q_j \rightarrow q_j e^{i\omega_j T}. \tag{1}$$

Meanwhile, the impulse and nonlinear phase-shift rules remain as before, so that

$$z_j \rightarrow \left(\gamma z_j + c \frac{z_j}{|z_j|}\right) e^{if(|z_j|)}. \tag{2}$$

The full map is the concatenation of Eqs. (1) and (2).

In practice, one starts with the phasors z_j, transforms to the q_j, applies Eq. (1), transforms back to the z_j, and finally applies Eq. (2). Therefore, the free propagation can be conveniently written as a matrix product

$$\tilde{\mathbf{z}} \rightarrow \mathbf{S}^{-1} \mathbf{D} \mathbf{S} \tilde{\mathbf{z}}$$

where $\mathbf{S}$ transforms the phasors to normal mode coordinates, $\mathbf{D}$ propagates the dynamics for a time T, and $\mathbf{S^{-1}}$ transforms back to the original coordinates.

The case of immediate interest involves two identical oscillators. Their phasors can be written as

$$\tilde{\mathbf{z}} = \begin{pmatrix} z_1 \\ z_2 \end{pmatrix},$$

which makes the relevant matrices

$$\mathbf{S} = \frac{\mathbf{1}}{\sqrt{\mathbf{2}}} \begin{pmatrix} 1 & 1 \\ 1 & -1 \end{pmatrix} = \mathbf{S}^{-1}$$

and

$$\mathbf{D} = \begin{pmatrix} e^{i\omega_+ T} & 0 \\ 0 & e^{i\omega_- T} \end{pmatrix} = \begin{pmatrix} \alpha & 0 \\ 0 & \beta \end{pmatrix},$$

so that

$$\begin{pmatrix} z_1 \\ z_2 \end{pmatrix} \rightarrow \frac{1}{2} \begin{pmatrix} \alpha + \beta & \alpha - \beta \\ \alpha - \beta & \alpha + \beta \end{pmatrix} \begin{pmatrix} z_1 \\ z_2 \end{pmatrix}. \tag{3}$$

Here, ω_+ and ω_- are the normal mode frequencies for the in-phase and antiphase modes, respectively.

The full map is the concatenation of Eqs. (2) and (3). For different choices of parameters, simulations of the map show three prominent regimes: coexisting in-phase and antiphase (periodic) states, a globally attracting in-phase state, or a globally attracting antiphase state. Figure 2 shows an example of what one sees as the quantity f varies. (Recall that f describes how the amplitude depends on frequency.) Each point corresponds to a single run, with randomly chosen initial phases, and an evolution time of 300 iterations. The final state was counted as in-phase if the phasors had a phase difference less than 0.001 over the last 100 iterations. It was counted as antiphase if the phase difference remained within 0.001 of π.

In order to sort out the conditions under which one or another of these dynamical regimes is predicted, we next perform a linear stability analysis of the iterative map.

III. ANALYSIS OF THE MAP

A. In-phase and antiphase fixed points

The full map has fixed point solutions representing in-phase and antiphase periodic solutions. The in-phase state is found by setting $z_1 = z_2$. Calling this common value z_0, the free running map (3) implies

$$z_0 \rightarrow e^{i\omega_+ T} z_0.$$

Composing this with Eq. (2) implies (for a fixed point)

$$z_0 = \left(\gamma z_0 + c \frac{z_0}{|z_0|} \right) e^{if(|z_0|)} e^{i\omega_+ T} \tag{4}$$

so that

$$1 = \left(\gamma + \frac{c}{|z_0|} \right) e^{if(|z_0|)} e^{i\omega_+ T}, \tag{5}$$

which involves only the magnitude of z_0. This complex equation determines the two real quantities $|z_0|$ and T; the phase of z_0 is left indeterminate.

To find the antiphase state(s), we set $z_1 = -z_2$. The free running map (3) then implies

$$z_0 \rightarrow e^{i\omega_- T} z_0.$$

Using this and Eq. (2), we arrive at the fixed point condition

$$1 = \left(\gamma + \frac{c}{|z_0|} \right) e^{if(|z_0|)} e^{i\omega_- T}. \tag{6}$$

Typically, the value of T is different for in-phase and antiphase states.

B. Stability of the in-phase state

To determine the stability of the in-phase state, we set

$$z_1 = z_0 + \eta_1 \quad \text{and} \quad z_2 = z_0 + \eta_2$$

and analyze the evolution of the small perturbations η_1 and η_2. As before, we propagate the full return map in two steps,
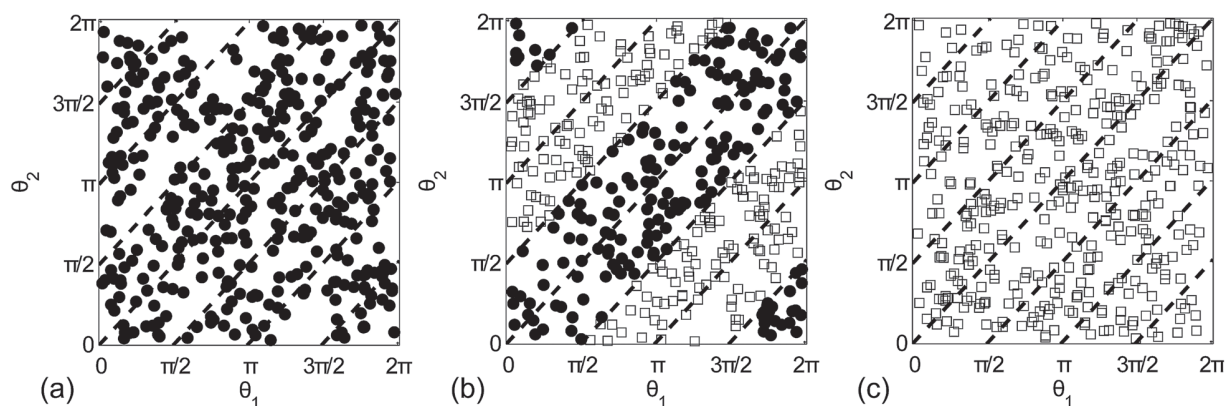

FIG. 2. Results of numerical simulations of the full map for different choices of $f(|z|)$. For each choice of initial phases θ_1 and θ_2, the system evolves into the in-phase state (circles) or the antiphase state (squares). Parameter values are $\omega_+ = 6.283$, $\omega_- = 5.970$, $c = 0.073$, $\gamma = 0.9$ and (a) $f(|z_j|) = -|z_j|^2/2$, (b) $f(|z_j|) = 0$, and (c) $f(|z_j|) = +|z_j|^2/2$.

first the impulsive kick (2), and then, the free evolution of the normal modes (3). We will write this as

$$z_j = z_0 + \eta_j \to \hat{z}_j = \hat{z}_0 + \hat{\eta}_j \to z_j' = z_0' + \eta_j',$$

so that the initial perturbation is η_j, after the first step it is $\hat{\eta}_j$, and after one iteration of the full map it is η_j'. Note that since z_0 corresponds to the fixed point of the full map, $z_0' = z_0$, but in general $\hat{z}_0 \neq z_0$.

Evolution under Eq. (2) takes η_j to $\hat{\eta}_j$ ($j = 1, 2$):

$$z_0 + \eta_j \to \hat{z}_0 + \hat{\eta}_j$$
$$= \left(\gamma z_0 + \gamma \eta_j + c \frac{z_0 + \eta_j}{|z_0 + \eta_j|} \right) e^{if(|z_0 + \eta_j|)}.$$

Expanding the various factors to first order in η_j yields

$$\hat{z}_0 + \hat{\eta}_j = \left(\gamma z_0 + c \frac{z_0}{|z_0|} \right) e^{if(|z_0|)}$$
$$+ \left\{ \gamma \eta_j + \frac{c}{2|z_0|} \left(\eta_j - \frac{z_0}{z_0^\star} \eta_j^\star \right) \right\} e^{if(|z_0|)}$$
$$+ \left(\gamma z_0 + \frac{c z_0}{|z_0|} \right) \cdot \frac{i|z_0|}{2} \left(\frac{\eta_j}{z_0} + \frac{\eta_j^\star}{z_0^\star} \right) f'(|z_0|) e^{if(|z_0|)}.$$

We can simplify this somewhat using Eq. (4), which results in

$$\hat{z}_0 + \hat{\eta}_j = \alpha^{-1} z_0 + \alpha^{-1} \eta_j$$
$$- \frac{c}{2|z_0|} \left(\eta_j + \frac{z_0}{z_0^\star} \eta_j^\star \right) e^{if(|z_0|)}$$
$$+ \frac{i|z_0|}{2\alpha} \left(\eta_j + \frac{z_0}{z_0^\star} \eta_j^\star \right) f'(|z_0|).$$

Since the stability properties are the same regardless of the choice of phase of z_0, without loss of generality we can choose z_0 to be real, i.e., $z_0 = \rho_0$. The last expression simplifies to

$$\hat{\rho}_0 + \hat{\eta}_j = \alpha^{-1} \rho_0 + \alpha^{-1} \eta_j$$
$$- \frac{c}{2\rho_0} e^{if(\rho_0)} \left(\eta_j + \eta_j^\star \right)$$
$$+ \frac{i\rho_0}{2\alpha} f'(\rho_0) \left(\eta_j + \eta_j^\star \right).$$

Next, we apply the free evolution map (3). This part of the map is linear, so we can consider its effect on the zeroth and first order terms separately. The zeroth order part merely recovers the fixed point, leaving the first order contribution:

$$\begin{pmatrix} z_1' \\ z_2' \end{pmatrix} = \frac{1}{2} \begin{pmatrix} \alpha + \beta & \alpha - \beta \\ \alpha - \beta & \alpha + \beta \end{pmatrix} \begin{pmatrix} \hat{z}_1 \\ \hat{z}_2 \end{pmatrix}$$
$$= \frac{1}{2} \begin{pmatrix} \alpha + \beta & \alpha - \beta \\ \alpha - \beta & \alpha + \beta \end{pmatrix} \begin{pmatrix} \hat{z}_0 + \hat{\eta}_1 \\ \hat{z}_0 + \hat{\eta}_2 \end{pmatrix}$$
$$= \frac{1}{2} \begin{pmatrix} \alpha + \beta & \alpha - \beta \\ \alpha - \beta & \alpha + \beta \end{pmatrix} \begin{pmatrix} \hat{z}_0 \\ \hat{z}_0 \end{pmatrix}$$
$$+ \frac{1}{2} \begin{pmatrix} \alpha + \beta & \alpha - \beta \\ \alpha - \beta & \alpha + \beta \end{pmatrix} \begin{pmatrix} \hat{\eta}_1 \\ \hat{\eta}_2 \end{pmatrix},$$

so that

$$\begin{pmatrix} \eta_1' \\ \eta_2' \end{pmatrix} = \frac{1}{2} \begin{pmatrix} \alpha + \beta & \alpha - \beta \\ \alpha - \beta & \alpha + \beta \end{pmatrix} \begin{pmatrix} \hat{\eta}_1 \\ \hat{\eta}_2 \end{pmatrix} \quad (7)$$

with

$$\hat{\eta}_j = \alpha^{-1} \eta_j - \frac{c}{2\rho_0} e^{if(\rho_0)} \left(\eta_j + \eta_j^\star \right) + \frac{i\rho_0}{2\alpha} f'(\rho_0) \left(\eta_j + \eta_j^\star \right).$$

Taking the modulus of Eq. (5), we have

$$1 = \left(\gamma + \frac{c}{\rho_0} \right) |\alpha|$$

so that

$$\hat{\eta}_j = \alpha^{-1} \eta_j - \frac{1}{2} \left(|\alpha|^{-1} - \gamma \right) \left(\eta_j + \eta_j^\star \right) + \frac{i\rho_0}{2\alpha} f'(\rho_0) \left(\eta_j + \eta_j^\star \right).$$

From Eq. (7), it follows that the symmetric and antisymmetric linear combinations decouple:

$$\begin{pmatrix} \eta_1' + \eta_2' \\ \eta_1' - \eta_2' \end{pmatrix} = \begin{pmatrix} \alpha & 0 \\ 0 & \beta \end{pmatrix} \begin{pmatrix} \hat{\eta}_1 + \hat{\eta}_2 \\ \hat{\eta}_1 - \hat{\eta}_2 \end{pmatrix}$$

so

$$(\eta_1' + \eta_2') = \left[1 - \frac{\alpha}{2} \left(|\alpha|^{-1} - \gamma \right) + \frac{i\rho_0}{2} f'(\rho_0) \right] (\eta_1 + \eta_2)$$
$$+ \left[-\frac{\alpha}{2} \left(|\alpha|^{-1} - \gamma \right) + \frac{i\rho_0}{2} f'(\rho_0) \right] (\eta_1^\star + \eta_2^\star)$$

and

$$(\eta_1' - \eta_2') = \left[\frac{\beta}{\alpha} - \frac{\beta}{2} \left(|\alpha|^{-1} - \gamma \right) + \frac{i\rho_0\beta}{2\alpha} f'(\rho_0) \right] (\eta_1 - \eta_2)$$
$$+ \left[-\frac{\beta}{2} \left(|\alpha|^{-1} - \gamma \right) + \frac{i\rho_0\beta}{2\alpha} f'(\rho_0) \right] (\eta_1^\star - \eta_2^\star).$$

Stability of the in-phase state is determined by the four eigenvalues of the matrix **M**:

$$\begin{pmatrix} \eta_1' + \eta_2' \\ \eta_1^{\star'} + \eta_2^{\star'} \\ \eta_1' - \eta_2' \\ \eta_1^{\star'} - \eta_2^{\star'} \end{pmatrix} = \mathbf{M} \cdot \begin{pmatrix} \eta_1 + \eta_2 \\ \eta_1^\star + \eta_2^\star \\ \eta_1 - \eta_2 \\ \eta_1^\star - \eta_2^\star \end{pmatrix},$$

Two of the eigenvalues are

$$\mu_1 = 1 \quad \text{and} \quad \mu_2 = \gamma |\alpha|,$$

while the other two are roots of the quadratic

$$\mu^2 - [(\gamma|\alpha| + 1)\Re e \xi - \rho_0 f'(\rho_0)\Im m \xi]\mu + \gamma|\alpha||\xi|^2 = 0, \quad (8)$$

where $\xi = \beta/\alpha = \Re e \xi + i\Im m \xi$. The in-phase state is stable provided none of the four eigenvalues lie outside the unit circle. Since physically realistic damping requires $\gamma < 1$ and $|\alpha| \leq 1$, the issue of stability rests with μ_3 and μ_4. The

coefficients of the quadratic are real, so these eigenvalues are either real or complex conjugates. The stability boundaries (in parameter space) can be determined as follows:

1. Case I: complex conjugate eigenvalues

In this case, the stability boundary is given by $|\mu_3| = |\mu_4| = 1$. From Eq. (8), it follows that the product $\mu_3\mu_4 = \gamma|\alpha||\xi|^2$, and so

$$|\xi|^2 = \frac{1}{\gamma|\alpha|}.$$

If $|\alpha|$ is held constant, this corresponds to a circle centered at the origin of the complex ξ plane with radius $\sqrt{1/(\gamma|\alpha|)}$. The in-phase state is unstable outside of this boundary.

2. Case II: real eigenvalues, $\mu > 0$

We can find the stability boundary by setting $\mu = +1$ in the quadratic. The stability boundary is given by

$$1 - (\gamma|\alpha| + 1)\Re e\xi + \rho_0 f'(\rho_0)\Im m\xi + \gamma|\alpha||\xi|^2 = 0.$$

This expression can be rearranged to get

$$(\Re e\xi - x_0)^2 + (\Im m\xi - y_0)^2 = r^2$$

where

$$x_0 = \frac{\gamma|\alpha| + 1}{2\gamma|\alpha|},$$
$$y_0 = -\frac{\rho_0 f'(\rho_0)}{2\gamma|\alpha|}, \tag{9}$$
$$\text{and} \quad r^2 = \frac{(\gamma|\alpha| - 1)^2 + \rho_0^2 f'(\rho_0)^2}{4\gamma^2|\alpha|^2}.$$

If $|\alpha|$ is held constant, the stability boundary is a circle centered at (x_0, y_0) with radius r when viewed on the complex ξ plane. The in-phase state is unstable inside this boundary.

3. Case III: real eigenvalues, $\mu < 0$

In this case, the stability boundary can be found by setting $\mu = -1$ in Eq. (8). The stability boundary is then given by

$$1 + (\gamma|\alpha| + 1)\Re e\xi - \rho_0 f'(\rho_0)\Im m\xi + \gamma|\alpha||\xi|^2 = 0,$$

which can be rearranged to get

$$(\Re e\xi - x_0)^2 + (\Im m\xi - y_0)^2 = r^2$$

where

$$x_0 = -\frac{\gamma|\alpha| + 1}{2\gamma|\alpha|},$$
$$y_0 = \frac{\rho_0 f'(\rho_0)}{2\gamma|\alpha|}, \tag{10}$$
$$\text{and} \quad r^2 = \frac{(\gamma|\alpha| - 1)^2 + \rho_0^2 f'(\rho_0)^2}{4\gamma^2|\alpha|^2}.$$

This boundary is a reflection about the origin (of the complex ξ plane) of the boundary derived for the $\mu = +1$ case. Inside this boundary, the in-phase state is unstable and the system is expected to undergo a period doubling bifurcation. However, this is unlikely in the case of the weakly coupled and symmetrically coupled, identical oscillators that are of interest in this paper. Under these conditions, the in-phase and antiphase modes are expected to have similar (complex) frequencies, so $\Re e\xi \sim +1$ and $\Im m\xi$ will be small and the system will operate far from this boundary.

C. Stability of the antiphase state

To determine the stability of the antiphase state, we set

$$z_1 = z_0 + \eta_1 \quad \text{and} \quad z_2 = -z_0 + \eta_2$$

and proceed as before. The calculation is similar to the in-phase case, and we omit it. It turns out that the first two eigenvalues are simply those previously determined (for the in-phase state) except for the exchange of α and β, i.e.,

$$\mu_1 = 1 \quad \text{and} \quad \mu_2 = \gamma|\beta|$$

while μ_3 and μ_4 are the roots of

$$\mu^2 - \left[(\gamma|\beta| + 1)\Re e\xi^{-1} - \rho_0 f'(\rho_0)\Im m\xi^{-1}\right]\mu + \gamma|\beta||\xi|^{-2} = 0$$

where $\xi = \beta/\alpha$. Since $|\beta| < 1$, stability hinges on whether μ_3 and μ_4 have modulus less than one. There are three cases:

1. Case I: complex conjugate eigenvalues

In this case, the stability boundary is given by $|\mu_3| = |\mu_4| = 1$, and from the quadratic we have $\mu_3\mu_4 = \gamma|\beta||\xi|^{-2}$, so that

$$|\xi|^2 = \gamma|\beta|.$$

If $|\beta|$ is held fixed, this corresponds to a circle in the complex ξ plane centered at the origin with radius $\sqrt{\gamma|\beta|}$. The antiphase state is unstable inside of this boundary.

2. Case II: real eigenvalues, $\mu > 0$

Setting $\mu = +1$ in the quadratic yields

$$1 - (\gamma|\beta| + 1)\Re e\xi^{-1} + \rho_0 f'(\rho_0)\Im m\xi^{-1} + \gamma|\beta||\xi|^{-2} = 0,$$

which can be rearranged to read

$$(\Re e\xi - x_0)^2 + (\Im m\xi - y_0)^2 = r^2$$

where

$$x_0 = \frac{1}{2}(\gamma|\beta| + 1),$$
$$y_0 = \frac{1}{2}\rho_0 f'(\rho_0), \tag{11}$$
$$\text{and} \quad r^2 = \frac{1}{4}\left[(\gamma|\beta| - 1)^2 + \rho_0^2 f'(\rho_0)^2\right].$$

The antiphase state is unstable inside of this boundary. If $|\beta|$ is held fixed, the stability boundary is a circle in the complex ξ plane, centered at (x_0, y_0) and with radius r.

3. Case III: real eigenvalues, $\mu < 0$

Setting $\mu = -1$ in Eq. (8), we get

$$1 + (\gamma|\beta| + 1)\Re e \xi^{-1} - \rho_0 f'(\rho_0)\Im m \xi^{-1} + \gamma|\beta||\xi|^{-2} = 0,$$

which can be rearranged to get

$$(\Re e \xi - x_0)^2 + (\Im m \xi - y_0)^2 = r^2$$

where

$$x_0 = -\frac{1}{2}(\gamma|\beta| + 1),$$

$$y_0 = -\frac{1}{2}\rho_0 f'(\rho_0), \qquad (12)$$

$$\text{and} \qquad r^2 = \frac{1}{4}\left[(\gamma|\beta| - 1)^2 + \rho_0^2 f'(\rho_0)^2\right].$$

As in the case of the stability boundary of the in-phase state for $\mu = -1$, this result is just a reflection about the origin of the stability boundary for antiphase state in the $\mu = +1$ case. The antiphase state is unstable inside of this circle, but again this regime of operation will be irrelevant for our discussion of weakly coupled clock/metronome systems where the in-phase and antiphase modes have similar frequencies.

As an illustration of these stability results, consider fixing the parameters γ, β, and ρ_0—the single oscillator damping parameter, the antiphase normal mode damping factors, and the steady state amplitude, respectively—and otherwise allowing $\xi = \beta/\alpha = e^{i(\omega_- - \omega_+)T}$ to vary. We can plot the stability boundaries in the complex ξ plane. Suppose we take $\gamma = \beta = 0.95$ and $\rho_0 = 1$. In principle, we also need to specify the amplitude-dependent frequency function $f(\rho)$ and calculate its derivative at the fixed point, but for now we just let $f'(\rho_0)$ be a parameter which we will make progressively

more negative, corresponding to a pendulum-like slowing with increasing amplitude. Figure 3 shows what happens to the stability boundaries of the in-phase and antiphase states as we vary $f'(\rho_0)$.

The stability boundaries corresponding to the complex conjugate eigenvalues for the in-phase and antiphase states appear as roughly circular arcs of radii ~ 1.05 and ~ 0.95. For $f'(\rho_0) = 0$, the stability boundaries corresponding to the real eigenvalues appear as bumps on the larger arcs. One of these boundaries is circular since $|\beta|$ is held fixed. Figure 3 shows that there are regions of the complex ξ plane where only the in-phase state is stable, regions where only the antiphase state is stable, and regions where both attractors are stable and initial conditions will determine the final state of the system. For large values of $f'(\rho_0)$, the boundaries cross each other and a region where neither state is stable emerges.

IV. PLATFORM-COUPLED CLOCKS AND METRONOMES

We now present an extended example, intended to allow us to revisit Huygens' original observations, its recreation by Bennett *et al.*, and the experiments of Pantaleone. To draw a quantitative connection between the map model and an actual physical system requires extracting the parameters ω_+, ω_-, γ, c, and the function f. The first two are the (complex) normal mode frequencies, and as we will show below, can be calculated in a straightforward way from the small oscillation limit. The other quantities are properties of a single oscillator and are likely more easily determined from measurements rather than calculating them from first principles. In particular, combining measurements of the steady state amplitude and the relaxation rate to the steady state allow one to determine the pair γ and c; meanwhile, measurements of how the steady state frequency varies with amplitude allows one to extract f, although for some cases (e.g., the plane pendulum) this may be calculated analytically.

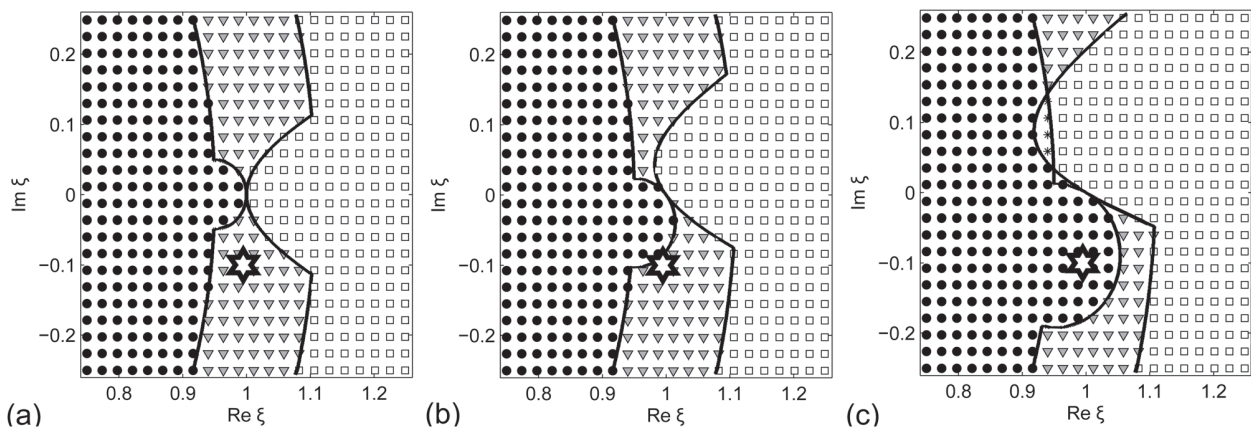Figure 1 shows the relevant schematic. The equations of motion are[6]

FIG. 3. Stability diagram plotted in the complex ξ plane for $\gamma = \beta = 0.95$ and $\rho_0 = 1$ (a) $f'(\rho_0) = 0$, (b) $f'(\rho_0) = -0.08$, and (c) $f'(\rho_0) = -0.25$. Circles correspond to values of ξ where only the in-phase state is stable. Squares correspond to values of ξ where only the antiphase state is stable. Triangles correspond to values of ξ for which the coexistence of in-phase and antiphase attractors is predicted. The asterisks in (c) mark values of ξ for which neither synchronized state is stable. The star marks a point where the in-phase and antiphase modes are equally damped but the frequency of the in-phase mode is higher.

$$\frac{d^2\phi_j}{dt^2} + b\frac{d\phi_j}{dt} + \frac{g}{\ell}\sin\phi_j = -\frac{1}{\ell}\frac{d^2X}{dt^2}\cos\phi_j + F_j$$

$$(M+2m)\frac{d^2X}{dt^2} + B\frac{dX}{dt} = -m\ell\frac{d^2}{dt^2}(\sin\phi_1 + \sin\phi_2)$$

where ϕ_j is the angular displacement of the jth pendulum, b is the pivot damping coefficient, g is the acceleration due to gravity, ℓ is the pendulum length, X is the linear displacement of the platform, F_j is the impulsive drive, M is the platform mass, m is the pendulum mass, and B is the platform damping coefficient. These same equations can be used if the pendulums are replaced by metronomes, as in the system studied by Pantaleone.[7] Introducing a scaled position $Y = X/\ell$ and time $\tau = t\sqrt{g/\ell}$, the governing equations can be put into non-dimensional form

$$\frac{d^2\phi_j}{d\tau^2} + 2\tilde{\gamma}\frac{d\phi_j}{d\tau} + \sin\phi_j = -\frac{d^2Y}{d\tau^2}\cos\phi_j + \tilde{F}_j$$

$$\frac{d^2Y}{d\tau^2} + 2\Gamma\frac{dY}{d\tau} = -\mu\frac{d^2}{d\tau^2}(\sin\phi_1 + \sin\phi_2) \tag{13}$$

where

$$\mu = \frac{m}{M+2m},$$

$$\tilde{\gamma} = \frac{b}{\sqrt{\ell/4g}}, \tag{14}$$

$$\text{and} \qquad \Gamma = B\sqrt{\ell/4g}/(M+2m).$$

Instead of looking at the escapement mechanism in detail (see, e.g., the paper by Lepschy *et al.*[14]), we use a modified version of the kick rule used by Bennett *et al.* When a pendulum is at the bottom of its swing, we apply a kick that mimics the two-part action of the escapement by first reducing the speed of the pendulum by factor γ as the escapement engages and then applying a fixed impulse c in the direction of the motion, i.e.,

$$\left|\frac{d\phi}{d\tau}\right| \rightarrow \gamma\left|\frac{d\phi}{d\tau}\right| + c.$$

In particular, we have chosen to kick the pendulum at the bottom of its swing to ease comparison with the results from the map. The current formulation of the map assumes that the kick changes the amplitude but not the phase of the phasors, although it can be generalized for more complicated kick rules.

The complex normal mode frequencies can be calculated by considering the small angle regime of the unforced system and introducing sum and difference coordinates $\sigma = \phi_1 + \phi_2$ and $\delta = \phi_1 - \phi_2$, so that

$$\frac{d^2\delta}{d\tau^2} + 2\tilde{\gamma}\frac{d\delta}{d\tau} + \delta = 0$$

$$\frac{d^2\sigma}{d\tau^2} + 2\tilde{\gamma}\frac{d\sigma}{d\tau} + \sigma = -2\frac{d^2Y}{d\tau^2} \tag{15}$$

$$\frac{d^2Y}{d\tau^2} + 2\Gamma\frac{dY}{d\tau} = -\mu\frac{d^2\sigma}{d\tau^2}.$$

It follows at once from the top equation that the antiphase normal mode has frequency

$$\omega_- = \sqrt{1-\tilde{\gamma}^2} + i\tilde{\gamma} \approx 1 + i\tilde{\gamma}, \tag{16}$$

where the last expression is valid for small pivot damping $\tilde{\gamma} \ll 1$. The other normal mode frequencies are roots of

$$(1-2\mu)\omega^3 - 2i(\tilde{\gamma}+\Gamma)\omega^2 - (1+4\tilde{\gamma}\Gamma)\omega + 2i\Gamma = 0.$$

One can show that one root is imaginary. This non-oscillatory mode corresponds to overdamped translational motion of the platform. (In the limit $\Gamma \rightarrow 0$, it represents uniform translation of the system.) The other normal mode corresponds to the in-phase state. The general solution for ω_+ is cumbersome, but for small coupling and pivot damping ($\mu, \tilde{\gamma} \ll 1$), we can expand the in-phase mode frequency to first order, with result

$$\omega_+ = 1 + \frac{\mu + i(\tilde{\gamma} + 2\mu\Gamma + 4\tilde{\gamma}\Gamma^2)}{1+4\Gamma^2}, \tag{17}$$

The in-phase mode has larger (real) frequency than the antiphase mode, and larger damping.

We are now in a position to see what the iterative map predicts for this system. Consider first the case of small amplitude oscillations and negligible platform damping $\Gamma \approx 0$. Then, the in-phase and antiphase states are essentially equally damped, but the in-phase state oscillates faster (i.e., its frequency has the larger real part). This means that in Fig. 3, the parameter ξ lies on the unit circle and in the fourth quadrant, as indicated by the six-pointed star. Both in-phase and antiphase states are stable. Figure 2(b) shows that, in this limit, the two attractors have nearly equal basin sizes.

Now imagine increasing the size of the impulsive force, so that the amplitude of the final states likewise increases. The amplitude-dependent phase shift becomes increasingly important (i.e., the map parameter f' becomes increasingly negative). The other map parameters are unchanged; in particular, ξ remains the same. As we see from Fig. 3, the antiphase stability boundary moves closer to the operating point and eventually crosses it, rendering the antiphase state unstable and the in-phase states globally attracting.

This behavior is borne out by numerical simulations of the ordinary differential equations (13). Figure 4 shows the eventual fate of various initial conditions for three different values of forcing strength (and all other system parameters held fixed). In all cases, the platform was initially at rest and the pendulums were started with equal energy but random phases θ_1 and θ_2. To the extent possible, we chose parameter values corresponding to the experiments reported in Ref. 6. We integrated the equations for approximately 300 oscillations. The final state was counted as in-phase if $|\phi_1 - \phi_2|$ remained less than 0.01 radians over the last several periods. Similarly, the final state was counted as antiphase if the angular difference remained within 0.01 radians of π. Trajectories that did not satisfy either condition within the allotted integration time are represented by triangles.
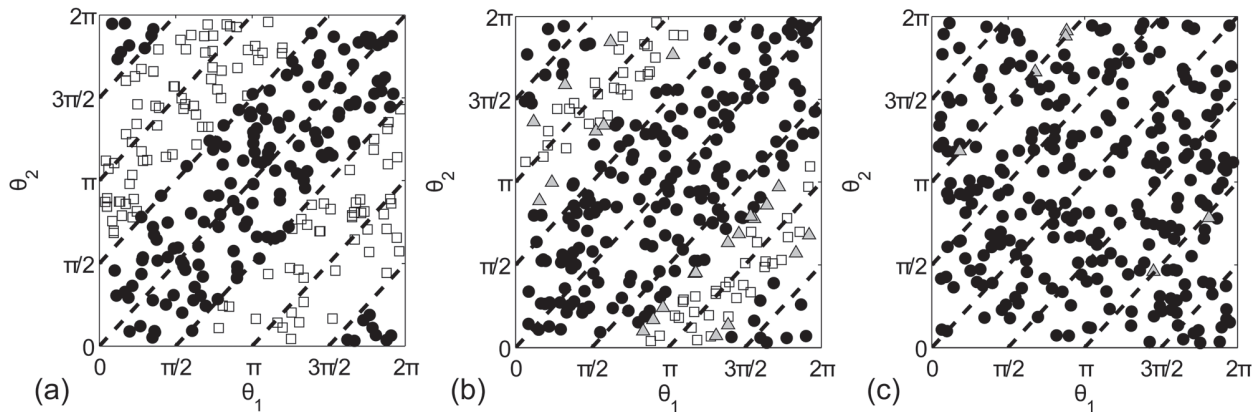
FIG. 4. Results of numerical simulations of Eqs. (13) for different levels of driving strength. For each initial condition, the system evolves into the in-phase state (circles), the antiphase state (square), or fails to reach either as defined in the text (triangles). Parameter values are $\Gamma = 0$, $\tilde{\gamma} = 1.63 \times 10^{-4}$, $\mu = 7.5 \times 10^{-3}$, $\gamma = 0.97$. (a) c = 0.0025, (b) c = 0.0065, and (c) c = 0.0085.

Figure 4 shows a clear progression. For weak driving, and hence small amplitude, in-phase and antiphase attractors coexist and their basins sizes are equal. As the driving strength increases, the in-phase basin grows at the expense of the antiphase basin. Eventually, the antiphase basin disappears and the in-phase state is globally attracting. Physically, one is seeing the effect of the amplitude-dependent oscillation frequency, a factor which becomes increasingly important for the pendulum (i.e., the frequency shifts more strongly the larger the amplitude).

Now, consider a second scenario. As before, begin in the limit of low drive and zero platform damping, so the in-phase and antiphase attractors coexist on a nearly equal footing. We now increase Γ, keeping the drive strength c (and all other parameters) fixed. Because the drive remains small, the large-amplitude phase shift parameter plays no role here. On the other hand, while the antiphase normal mode frequency does not change, the in-phase frequency does: from Eq. (17), the imaginary part of ω_+ grows, corresponding to an increasingly damped mode. This disfavors the in-phase state. In terms of the map parameters, the modulus of ξ grows. As can be seen from Fig. 5, the operating point moves closer to the stability

boundary of the in-phase state, and eventually crosses it, beyond which point the antiphase state is the only attractor.

This is precisely what we see in simulations of the differential equations (see Fig. 6). For small platform damping, the in-phase and antiphase states have essentially equal sized basins of attraction. When the platform damping parameter is increased to a value $\Gamma = 0.2$, the in-phase state has lost basin size to the antiphase state. By the time $\Gamma = 0.5$, the in-phase state has lost stability, and all initial conditions lead to the antiphase final state.

V. DISCUSSION

Our model is a generic description incorporating a few basic processes. First, at the single oscillator level, rule (2) describes a limit cycle with amplitude and relaxation rate determined by the parameters c and γ, and an amplitude-dependent frequency through the function f. The latter in particular plays a crucial role in the behavior of the coupled system. Meanwhile, coupling between the oscillators leads to two important processes: the splitting of frequencies for the collective modes, and damping of these modes. These
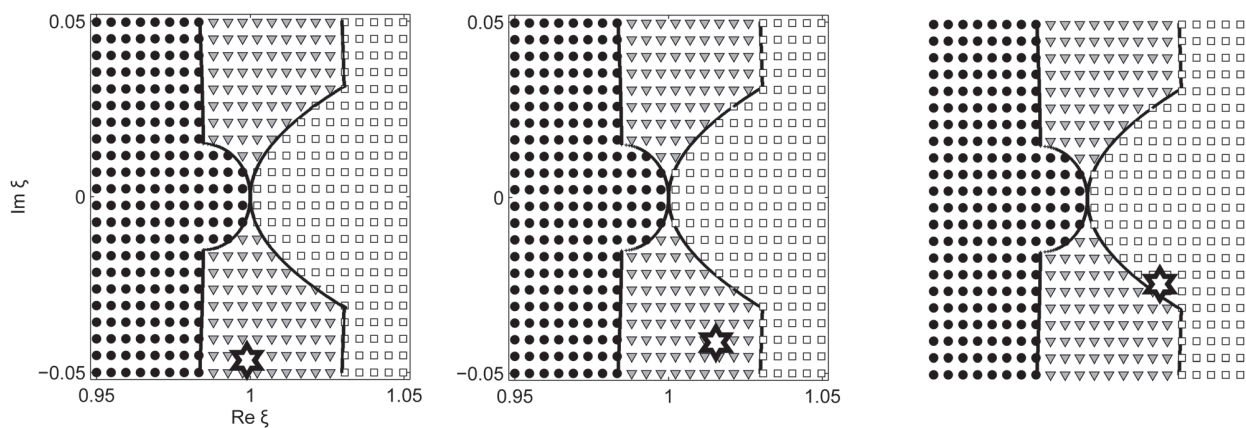

FIG. 5. Map stability diagram plotted in the complex ξ plane for $\gamma = 0.98$, $f'(\rho_0) = 0, 5$, $\rho_0 = 1$. α and β were calculated using the frequencies determined using Eqs. (17) and (16) for $\tilde{\gamma} = 1.63 \times 10^{-4}$, $\mu = 7.5 \times 10^{-3}$, and (a) $\Gamma = 0$, (b) $\Gamma = 0.2$, and (c) $\Gamma = 0.5$. The star shows the evolution of ξ as Γ is increased.
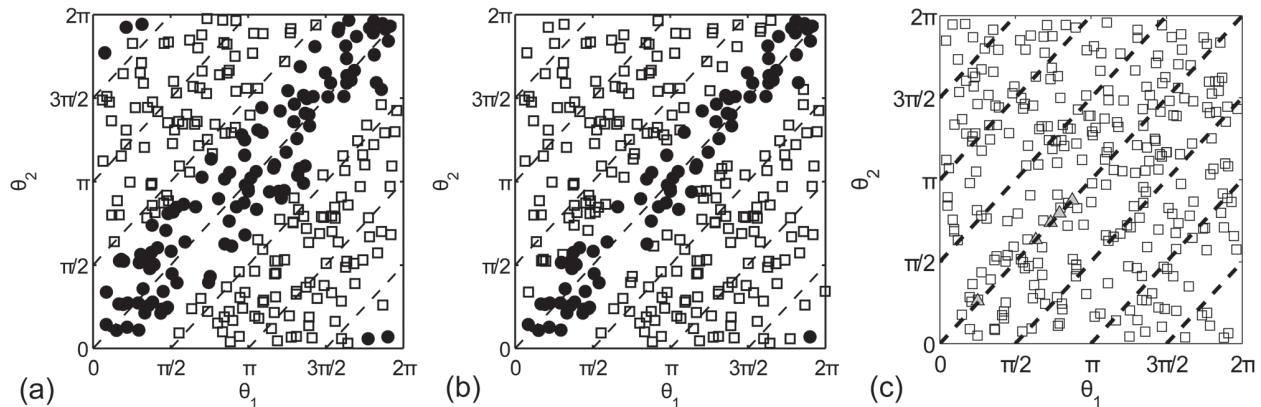
FIG. 6. Results of numerical simulations of Eqs. (13) for different levels of platform damping. For each initial condition, the system evolves into the in-phase state (circles), the antiphase state (squares), or fails to reach either within the allotted integration time (triangles). Parameter values are $\tilde{\gamma} = 1.63 \times 10^{-4}$, $\mu = 7.5 \times 10^{-3}$, $\gamma = 0.97$, $c = 0.0025$, and (a) $\Gamma = 0$, (b) $\Gamma = 0.2$, (c) $\Gamma = 0.5$.

effects are accounted for by the real and imaginary parts, respectively, of the complex frequencies ω_+ and ω_-.

The map model certainly represents a simplified view of any real system, and therein lies its utility. It provides a common perspective for comparing different problems. Admittedly, the differences between the experiments of Huygens, Bennett *et al.*, and Pantaleone are rather mild; nevertheless, the behavior of the latter is virtually the mirror image of the others. Our map model provides a natural platform for direct comparisons.

Simulations of the map show three prominent regimes: coexisting in-phase and antiphase (periodic) states, globally attracting in-phase state, and globally attracting antiphase state. The coexistence regime is typical for relatively low-amplitude, low-damping dynamics. Stability analysis confirms two distinct effects leading to single-attractor dominance. The first is rather obvious from a physical point of view: as the differential damping between the modes increases, the less-damped mode is favored. The second effect is not obvious: the larger the oscillator amplitude, the more one mode is favored over the other. Which is the favored mode? As seen in Fig. 2, if, as in the case of a pendulum, the oscillator slows with increasing amplitude, the higher-frequency mode is favored at larger amplitudes.

These observations provide us with a natural explanation of the various experiments. In Huygens' system, the supporting beam moved with difficulty, substantially damping the in-phase mode (but not the antiphase mode, see Eq. (16)). At the same time, Huygens' clocks employed a cycloidal-shaped boundary specifically designed to eliminate the usual amplitude-dependent frequency of a pendulum.[13] The experiments of Bennett *et al.* had no such boundary, but the actual pendulums' amplitudes remained small (about 9° as compared with Huygens' 20°), so again the effect, which could have stabilized the in-phase state, was absent.

The situation was reversed in Pantaleone's experiments. The platform damping was small (so neither mode was disadvantaged), but the amplitude-dependent frequency effect was substantial (favoring in-phase over antiphase). Moreover, we have an explanation for the "special conditions" under which the metronome system did show stable antiphase behavior.

First, when the supporting cylinders were put on a wet surface, this lead to increased platform damping, which pushed the system into the Huygens regime.

Pantaleone also reported that his metronomes synchronized to the antiphase state when they were operated at high frequency by removing their adjustable pendulum bobs. One can show that by removing the pendulum bobs, the effective coupling constant and the effective platform damping are increased; in the case of metronomes these are given by expressions similar, but not identical to Eq. (15). These changes increase the difference in ω_+ and ω_-. In the complex ξ plane, this corresponds to increases in both the real and imaginary parts of ξ, which moves the system away from the region where the in-phase state is globally attracting and into the region of coexistence.

There are additional predictions implied by the map model. For example, if the coupling mechanism were changed so that it coupled into the antiphase mode, any associated damping would favor the in-phase state (the opposite of Huygens' case). Other predictions follow from a kind of "reciprocity inherent in the model. The notion of "in-phase" or "antiphase" doesn't explicitly appear in the model. The only property distinguishing the competing collective modes is the frequency: our notation ω_+/ω_- was suggestive of in-phase/antiphase motion, but what actually matters is that ω_+ has the larger real part. In particular, if the coupling mechanism were altered so that the in-phase state had smaller real part, the tendency at large amplitude would be reversed: pendulum-type oscillators would favor antiphase motion at higher amplitudes (the opposite of Pantaleone's case). A final prediction holds for non-pendulum oscillators whose frequency increases with increasing amplitude, e.g., those with a hard spring Duffing nonlinearity. The preference for in-phase vs. antiphase is reversed: for platform coupled oscillators like those described by Eq. (13), the in-phase state is *destabilized* at higher amplitudes. This can be seen in Fig. 2(c), where the oscillation frequency increases with amplitude.

Finally, although in this paper, we focused on mechanical systems, our map model can be used to consider other kinds of oscillator systems, for example electrical oscillators or certain laser systems. The model also can be used to

describe larger arrays, and may serve as a useful tool for studying such problems in a unified way.

ACKNOWLEDGMENTS

[1]S. H. Strogatz, *Sync: How Order Emerges From Chaos In the Universe, Nature, and Daily Life* (Hyperion, New York, NY, 2004).

[2]I. I. Blekhman, *Synchronization in Science and Technology* (American Society of Mechanical Engineers, New York, NY, 1998).

[3]A. Pikovsky, M. Rosenblum, and J. Kurths, *Synchronization*: *A Universal Concept in Nonlinear Sciences, Cambridge Nonlinear Science Series* (Cambridge University Press, Cambridge, UK, 2003).

[4]C. Huygens, *Oeuvres complètes de Christiaan Huygens*, Vol. 5 (Martinus Nijhoff, The Hague, 1893), pp. 241–262.

[5]C. Huygens, *Oeuvres complètes de Christiaan Huygens*, Vol. 17 (Martinus Nijhoff, The Hague, 1932), pp. 156–189.

[6]M. Bennett, M. F. Schatz, H. Rockwood, and K. Wiesenfeld, Proc. R. Soc. Lond. A **458**, 563 (2002).

[7]J. Pantaleone, Am. J. Phys. **70**, 992 (2002).

[8]H. Ulrichs, A. Mann, and U. Parlitz, Chaos **19**, 043120 (2009).

[9]R. Dilão, Chaos **19**, 023118 (2009).

[10]K. Czolczynski, P. Perlikowski, A. Stefanski, and T. Kapitaniak, Physica A **388**, 5013 (2009).

[11]K. Czolczynski, P. Perlikowski, A. Stefanski, and T. Kapitaniak, Prog. Theor. Phys. **122**, 1027 (2011).

[12]K. Czolczynski, P. Perlikowski, A. Stefanski, and T. Kapitaniak, Chaos **21**, 023129 (2011).

[13]C. Huygens, *Christiaan Huygens's the Pendulum Clock or Geometrical Demonstrations Concerning the Motion of Pendula As Applied to Clocks* (translated by R. Blackwell) (Iowa State University Press, Ames, IA, 1986).

[14]A. M. Lepschy, G. A. Mian, and U. Viaro, IEEE Trans. Educ. **35**, 3 (1992).